AJNR

Fast multiphase MR imaging of aqueductal CSF flow: 1. Study of healthy subjects.

L Ciraolo, M Mascalchi, M Bucciolini and G Dal Pozzo

AJNR Am J Neuroradiol 1990, 11 (3) 589-596
http://www.ajnr.org/content/11/3/589

Fast Multiphase MR Imaging of Aqueductal CSF Flow: 1. Study of Healthy Subjects

Lilina Ciraolo[1]
Mario Mascalchi
Marta Bucciolini
Giancarlo Dal Pozzo

Gradient-echo MR sequences are more sensitive to flow phenomena than spin-echo sequences are. We investigated aqueductal CSF flow by fast multiphase imaging. Fast multiphase imaging offers the opportunity to perform a dynamic study of fluid motion that is synchronous with the cardiac cycle. A section perpendicular to the cerebral aqueduct was imaged in 18 healthy volunteers. Serial, gated (every 50 msec from the ECG R wave), flow-compensated modulus images with 70°-flip-angle excitation pulses were obtained with a single acquisition. The behavior vs time of CSF signal in the aqueduct was compared with that in the lateral ventricles. The former showed a peak at 0.47 ± 0.1 fractions of a heart cycle after the R wave. No periodicity with the heart rate was observed for the ventricular CSF signal intensity. The mean CSF signal intensity in the aqueduct was found to range from about twice to three times that in the lateral ventricles over a cardiac cycle.

Fast multiphase imaging is a sensitive and practical sequence for the MR investigation of aqueductal CSF flow. Its potential in patients with hydrocephalus is studied in a companion article.

AJNR **11:589–596, May/June 1990**

MR imaging is markedly sensitive to flow phenomena and, owing to its noninvasive nature, appears ideal for the investigation of CSF circulation physiology. On conventional modulus spin-echo (SE) images, a lower signal intensity in the cerebral aqueduct of healthy subjects, as compared with that in the lateral ventricles, has been noted and attributed to both time-of-flight and phase-shift effects, which determine the signal intensity of flowing fluids [1, 2]. Moreover, with cardiac gating, the magnitude of this "aqueductal signal void" has been found to vary within the heart cycle, being more pronounced in systolic phases [3–5].

New gradient-echo sequences have recently been introduced that are more sensitive to flow phenomena than SE sequences are [6–10]. In fast multiphase imaging (FMI), serial images at different delay times from the R wave of the cardiac cycle can be obtained with short single acquisitions [11]. The opportunity FMI offers to perform a dynamic study of fluid motion that is synchronous with the heart pumping action prompted us to investigate aqueductal CSF flow with the use of this sequence in healthy volunteers.

Subjects and Methods

FMI Pulse Sequence

FMI, as displayed in Figure 1, consists of a series of small-angle excitation pulses given at short time intervals during a heart cycle; each echo signal is produced by gradient reversal. With the use of a 256 × 256 matrix, each pulse, triggered by the ECG R wave, is repeated 256 times and the image is obtained from the 256 echo signals corresponding to the same point of the heart cycle.

Received June 22, 1989; revision requested August 8, 1989; revision received September 28, 1989; accepted October 11, 1989.

Presented in part at the annual meeting of the Society of Magnetic Resonance in Medicine, Amsterdam, August 1989.

This work was supported in part by National Research Council grants 870102002 and 860154502 and the Ministero Pubblica Istruzione.

[1] All authors: Department of Clinical Physiopathology, University of Florence, Florence, Italy. Address reprint requests to M. Mascalchi, MR Unit, Radiodiagnostic Section, Department of Clinical Physiopathology, University of Florence, Viale Morgagni 85, 50134 Florence, Italy.

0195-6108/90/1103-0589

It can theoretically be deduced (see Appendix) that, assuming a steady laminar flow at a given flip angle, the FMI signal is markedly dependent on flow phenomena, increasing as a linear function of velocity up to a saturation level [10]. In addition, when increasing flip angles are used, a more and more marked flow-related enhancement is expected.

In previous phantom fluid studies detailed in the Appendix, we tested the dependence of FMI signal on flow rate and excitation pulse angle in the case of both continuous and pulsatile flow. The results of these investigations demonstrated that, whereas a substantial correlation between theoretical prediction of flow rate and experimental data can be found in the case of continuous flow, in the case of pulsatile flow, such as that known to occur in the cerebral aqueduct, gradient-echo imaging does not allow extrapolation of precise quantitative flow data from the MR signal intensity.

Subjects and Study Protocol

Eighteen healthy volunteers (11 women and seven men; mean age, 42.7 ± 13.3 years) were imaged on a standard 0.5-T MR scanner (Philips Gyroscan).

A preliminary sagittal multislice scan was obtained with an SE sequence, 350/30/2 (TR/TE/excitations), to visualize the cerebral aqueduct. Reconstruction was done by two-dimensional Fourier transform (2DFT) with a field of view of 250 × 250 mm. The matrix was composed of 256 × 256 pixels.

An ECG-gated oblique transverse single slice, perpendicular to the main axis of the aqueduct and passing through its midportion, was then imaged with an FMI sequence and reconstructed as above. This slice, 6 mm thick, affords a view of a posterior segment of the lateral ventricles as well.

A 70° flip angle and a 50-msec heart-phase interval were chosen because they represent a compromise between satisfactory flow-related enhancement and a detailed analysis of the signal during the cardiac cycle. Larger flip angles would have required the use of a longer heart-phase interval for acceptable magnetization to be achieved at the echo time. The shortest trigger delay from the R wave (15 msec) and the shortest echo time (15 msec) were used. A first-order flow compensation was applied; this consists of the addition of gradient pulses for correction of flow-related phase accumulation. In this way, rephasing is induced to compensate for constant-velocity motion.

The number of serial excitations for each subject was calculated according to the heart cycle (60/cardiac frequency [sec]), after subtracting the time needed for gradient loading (about 100 msec with our scanner). Actually, although FMI enables one to cover the entire cardiac cycle, the time required by the unit's hardware and software makes the interval between the last excitation of an FMI pulse train and the first one of the ensuing train (after the subsequent R wave) always longer than 50 msec, resulting in a much stronger signal in the first few frames. This effect diminishes progressively from frame to frame; in our setting, the magnetization steady state is reached, within an approximation of 2.5%, at the sixth excitation (see Appendix).

In order to obtain frames of uniform signal intensity over the entire cardiac cycle, we rejected the first five frames of the FMI sequence and, taking into account the subject's heart period, extended the FMI pulse train over two consecutive cardiac cycles by dropping every second R wave. Diastolic data—that is, findings within 200–300 msec from the R wave—were then measured from the first excitations, which, according to the subject's heart period, refer to the second cardiac cycle. In this way, an average of 20–25 serial images were acquired for each subject.

Although a constant cardiac rate was assumed during acquisition, it should be remembered that variations in cardiac frequency can cause a varying attribution of the aqueductal signal intensity to nearby frames. This effect is likely to flatten the curve of the aqueductal CSF signal vs time. A minimum heartbeat interval between two FMI pulse trains (60/cardiac frequency [sec] × 2) was inserted in order to avoid spurious excitations. The FMI acquisition took about 10 min.

Data Analysis

For all subjects, signal intensity within the cerebral aqueduct cross section and one of the lateral ventricles, the latter containing relatively stationary CSF, was measured with the use of a round region of

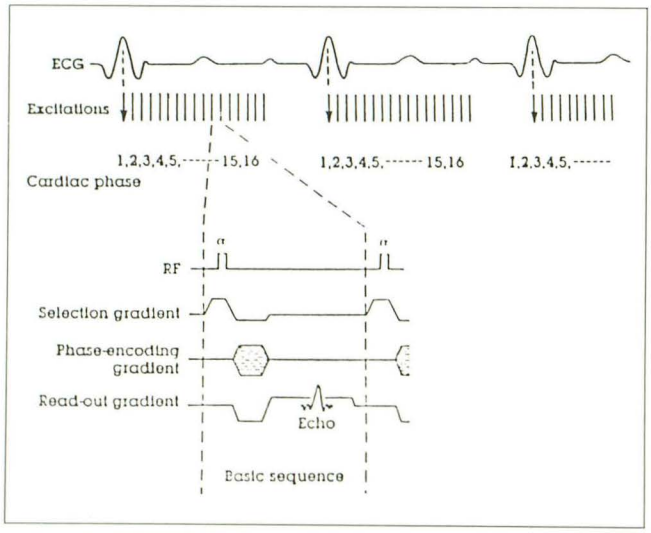

Fig. 1.—Fast multiphase MR pulse sequence [11]. α = RF pulse.

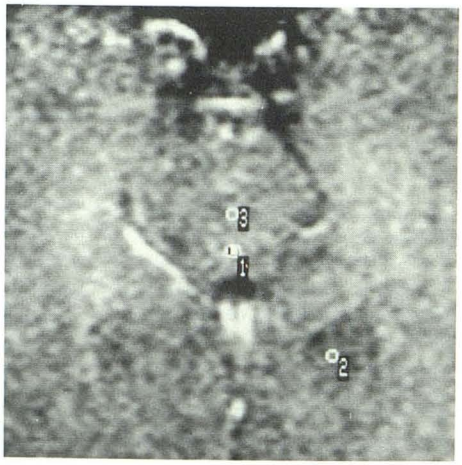

Fig. 2.—Fast multiphase MR display of mid aqueduct and posterior segment of lateral ventricles corresponding to delay time of 380 msec (frame 8). Circular regions of interest are selected within aqueduct (1), lateral ventricle (2), and median pons (3).

interest in each serial FMI image, starting from the sixth. A region of interest of equal size was selected in the pons providing a measurement of brain tissue (Fig. 2). The signal-intensity behavior in the aqueduct, lateral ventricles, and pons was analyzed vs the delay time from the R wave, in order to evaluate signal variations during the cardiac cycle.

Results

Fifteen serial FMI images (from the sixth to the 20th) of one of the subjects are shown in Figure 3. The corresponding signal intensities in the aqueduct, lateral ventricles, and pons are plotted vs delay time in Figure 4. Aqueductal signal intensity, appearing constantly higher as compared with that of the lateral ventricle and pons, quickly increases up to its maximum, occurring at a delay time of 380 msec from the R wave. A smooth decrease follows to 680 msec; thereafter, a new increase is observed starting a new cycle. Note that the second peak is lower than the first. The signal intensities in both the lateral ventricles and pons show minor fluctuations during the cardiac cycles without any appreciable periodicity. Moreover, whereas the signal intensity in the pons appears to be quite stable, that in the lateral ventricles shows a slight progressive decrease, which is observable for the aqueduct also. Similar relationships between signal intensities in the aqueduct, lateral ventricles, and pons vs delay time were observed in all the subjects.

The mean delay time from the R wave of the maximum aqueductal signal intensity was 379 ± 59 msec. By normalizing the delay of the maximum aqueductal signal to the duration of the cardiac cycle in each subject, the mean delay value could be expressed in fractions of cycle and was 0.47 ± 0.06. The (mean) maximum value of the aqueduct/lateral ventricle signal-intensity ratio was 3.23 ± 0.40 (range, 2.41–3.84); the minimum was 1.71 ± 0.26 (range, 1.26–2.14).

Discussion

The investigation of the physiology of CSF dynamics in humans has been hampered considerably by the invasiveness of the available techniques such as intracranial pressure monitoring, cineventriculography, and cisternography. However, a periodic increase of the endoventricular CSF pressure occurring at a mean delay time of 100 msec from the cardiac R wave, followed by a plateau phase of about 250 msec, was reported by Bering [12] in a group of neurosurgical patients and confirmed by Laitinen [13] in parkinsonian patients who underwent thalamotomy. Whereas it is widely accepted that these variations correspond to the transmission to the CSF of the systolic arterial pressure pulse wave, the origin of this transmission is debated, including the choroid plexuses of the cerebral ventricles [12], the large arteries of the base of the brain [13], the craniospinal venous system [14], and the parenchymal capillary-venous junction [15]. In 1966, using air- and oil-contrast cineventriculography, du Boulay [16] demonstrated the pulsatility of the aqueductal CSF flow, a caudad flow occurring in systole and a reversal; that is, cranial flow, occurring in diastole. The to-and-fro motion of the aqueductal CSF, synchronous with the cardiac cycle, has recently been demonstrated noninvasively with phase SE MR [17].

A definite flow-related variation in signal intensity in the cerebral aqueduct during the cardiac cycle was reported for the first time by Bergstrand et al. [3] using a cardiac-gated inversion-recovery (IR) sequence. This variation in the aqueductal CSF signal intensity in normal subjects was subsequently confirmed by others using cardiac-gated SE modulus imaging, with a lower signal intensity corresponding to higher flow rates for the systolic images [4, 5]. All the above studies are limited by the need for repeated acquisitions at different delay times from the ECG R wave, which makes them impractical for clinical application.

Atlas et al. [18] recently reported that flowing CSF in the patent aqueduct is seen as high intensity on flow-compensated gradient-echo images. Aqueductal CSF hyperintensity, an expression of flow-related enhancement, was observed by us on FMI.

The periodic behavior of the aqueductal hyperintensity and the delay time of the flow peak we have observed complement the findings of other gated MR studies [3–5]. Given the theoretic linear relationship between gradient-echo signal enhancement and low flow rates, and the results of phantom studies performed by us (see Appendix) and others [10], these variations are expected to reflect closely corresponding flow variations during a cardiac cycle, presumably owing to changes in endoventricular CSF pressure.

Since the signal intensities of the aqueductal CSF we measured do not consider the actual direction of aqueductal flow, one would expect two peaks within a heart cycle, corresponding to systole and diastole with a zero point of flow reversal in between. The temporal resolution (50 msec) of the acquisition in our study is likely to prevent the display of such a behavior, implying omission of the inversion time and a smoothing of the two peaks of the cardiac cycle into one.

Moreover, in all subjects the peak of the aqueductal CSF signal intensity of the second heart cycle sampled was smaller than that of the first one (Fig. 4). This paralleled a progressive decrease in the signal intensity of the lateral ventricles, in contrast to a substantial stability in the signal of the brain tissue.

Speculations about the cause of this phenomenon can be suggested. It might be related to phase effects caused by an imperfect gradient reversal in the FMI sequence. Because of this, the magnetization will be progressively reduced after each subsequent excitation and, according to the heart-phase interval/T1 ratio, the effect will be more prominent for CSF compared with brain tissue given the longer T1 relaxation time of the former. Another possible explanation for the decrease in CSF signal intensity might be minor physiological variations in the heart period, causing a wrong attribution of signal intensity to each heart phase and progressive flattening of flow-related signal variations. This effect, however, does not explain the signal decrease in the stationary CSF in the lateral ventricles.

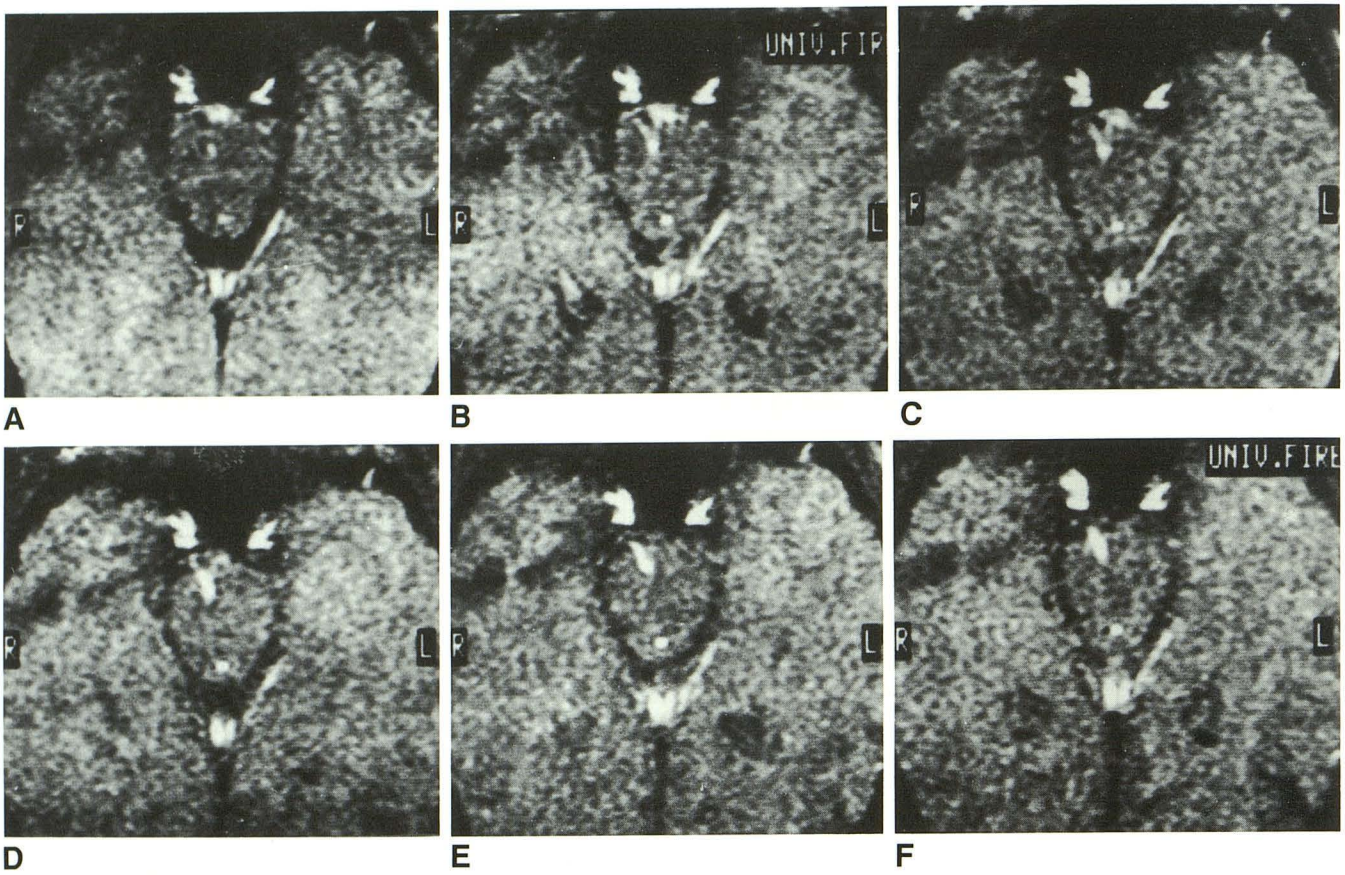

Fig. 3.—*A–O*, Fifteen serial (every 50 msec) fast multiphase gated MR images in a healthy volunteer. The first frame (*A*) corresponds to a delay time of 280 (trigger delay time + echo time + 250 msec) from the R wave, the last one (*O*) to a delay time of 980 msec.

The ideal goal in investigating aqueductal CSF dynamics would be to express the flow rates quantitatively. Both time-of-flight and phase effects strongly contribute to the flow signal on IR and SE modulus images; therefore, any evaluation of the aqueductal CSF velocity directly from these IR or SE modulus images—that is, by taking into account only the time-of-flight effects—cannot be accurate [5].

Concerning the possibility of extrapolating quantitative velocity values from the FMI signal intensity measured in the aqueduct, we have considered the results of previous phantom flow studies performed at our institution analyzing the relationship between flow rates and signal in the case of both continuous and pulsatile flow. The results for continuous flow showed a substantial linear correlation between experimental data and theoretical predictions, confirming the results of a recent study [10]. In the case of pulsatile flow, an analogous correspondence could not be found, which casts doubts on the precision of the velocity values that can be calculated using FMI in such a case.

Since the extrapolation of quantitative velocity values of aqueductal CSF flow from MR images has several additional problems, such as the irregular shape of the conduit and the periodic reversal of flow during the cardiac cycle, both of which may induce turbulence, and is based on the assumed absence of motion of the ventricular CSF, we have concluded that a quantitative approach cannot be pursued. This notwithstanding, our investigation indicates that FMI, by enhancing the flow contrast far more than is possible with SE, is a sensitive and practical sequence for the study of aqueductal CSF dynamics. Its potential as a noninvasive tool for the investigation of aqueductal CSF flow pathophysiology in patients with hydrocephalus is the subject of a companion article [19].

Appendix

Theoretical Background

FMI is more sensitive than SE to flow phenomena because the FMI signal shows a much stronger dependence on velocity. Reasons for this behavior can be summarized:

1. The signal caused by spin inflow in the selected slice is markedly enhanced with respect to that of stationary tissues because the magnetization of the latter remains strongly saturated during the short repetition time.

2. Outflowing spin magnetization is not disturbed by any additional

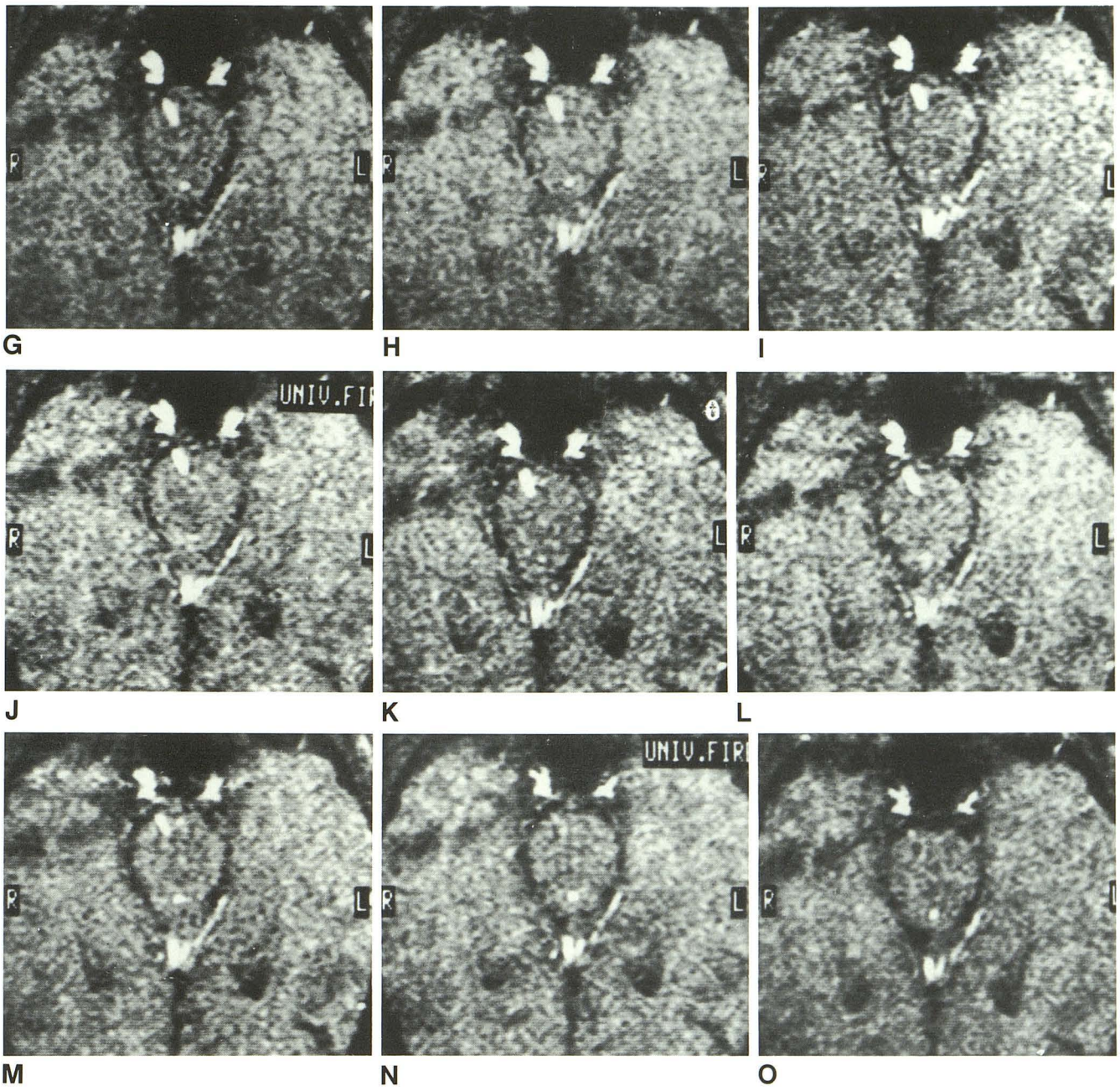

Fig. 3.—Continued.

selective pulse (the 180° inversion pulse is not present), and therefore it contributes fully to the echo signal.

3. The short duration of the selection, readout, and preparation gradients causes a small dephasing of flowing spins, as compared with SE.

An analytical expression for the FMI signal dependence on flow can be derived by considering the fraction R(t) of spins excited by the RF α pulse and still present in the selected slice after a time t. In the case of laminar flow, assuming a parabolic velocity profile over the cross section of the vessel, and integrating the contributions of infinitesimal circular rings, R(t) is

$$(1/\pi\ Ro^2) \int_0^{R_o} [1 - v(r)t/\Delta z]2\pi r dr$$

if $V_{max} \leq \Delta z/t$, and

$$(1/\pi\ Ro^2) \int_{r_o}^{R_o} [1 - v(r)t/\Delta z]2\pi r dr$$

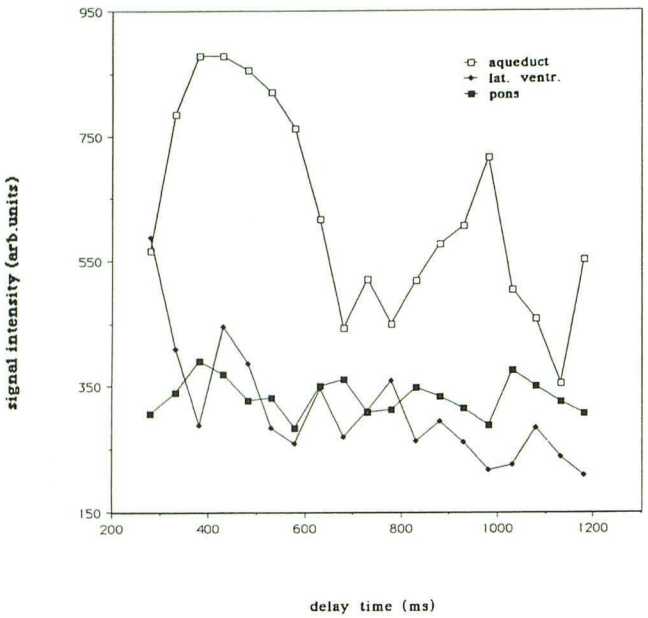

Fig. 4.—Plot of signal intensity in arbitrary (arb.) units in aqueduct, lateral ventricle (lat. ventr.), and pons vs delay time from R wave, corresponding to images in Fig. 3. Aqueductal signal intensity quickly increases up to its maximum, occurring at a delay of 380 msec. A smooth decrease follows to 680 msec; thereafter, a new increase is observed starting a new cycle.

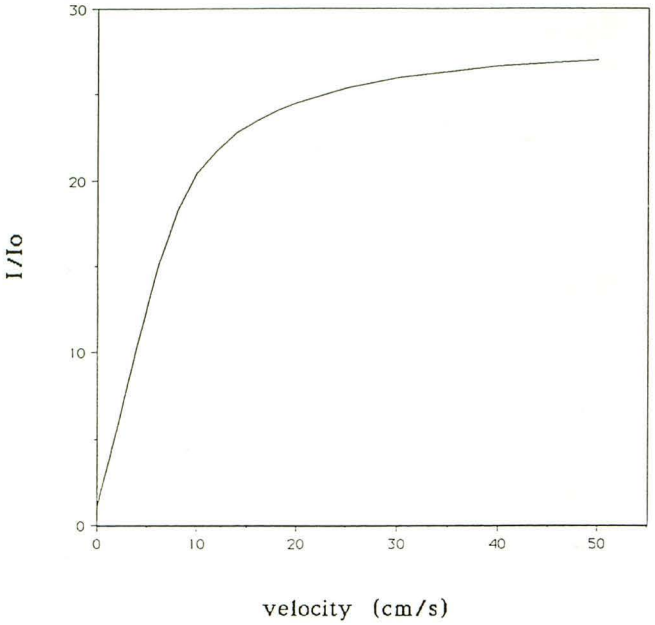

Fig. 5.—Plot of theoretical behavior of fast multiphase MR signal, normalized to signal of static fluid (I/Io), vs mean velocity for these acquisition parameters: slice thickness = 6 mm; heart phase interval = 50 msec; T1 (CSF) ≅ 2000 msec; flip angle = 70°.

if $V_{max} \geq \Delta z/t$. Ro is the vessel's radius, Δz is the slice thickness, and $v(r_o)$ is the minimum velocity (equal to $\Delta z/t$) that allows a full replacement of spins in a time t.

If Io is the signal expected in the static conditions, when the magnetization has already reached a steady state after subsequent excitations, its equilibrium value will be

$$Io = k \{[1 - \exp(-\tau/T1)] \sin \alpha / [1 - \cos \alpha \exp(-\tau/T1)]\} \exp(-TE/T2). \quad (1)$$

This value is asymptotically reached more or less rapidly, depending on flip angle, relaxation times, and heart-phase interval (τ). In fact, by solving the Bloch equations, a recurrent formula for the signal following each excitation can be found:

$$I_{on} = I_o (n - 1) - I_{o1} (\cos \alpha)^{n-2} (1 - \cos \alpha) \exp[-(n - 1) \tau/T1],$$

where I_{on} is the signal detected after the n-th excitation, τ the heart-phase interval, and α the RF pulse.

For $\tau = 50$ msec, T1 ≅ 2000 msec, and $\alpha = 70°$, we have

$$(I_{o5} - I_{o6})/Io = 2.5\%.$$

Therefore, assuming for the static signal the expression 1 derived above, it follows that the flow signal I is

$$I = \{R(\tau)Io + [1 - R(\tau)]k \exp(-TE/T2)\},$$

where τ and TE are repetition time and echo time of each serial FMI

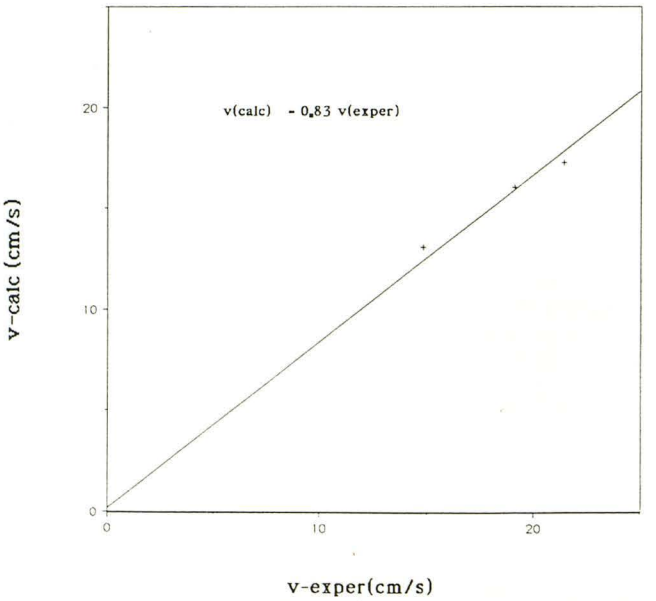

Fig. 6.—Comparison between flow rates (v) experimentally (exper) measured and those calculated (calc) from fast multiphase MR signal in phantom in the case of continuous flow. A 70° flip angle is considered. For other acquisition parameters, see text. Agreement within 17% is found.

excitation, respectively, and T1 and T2 are the spin-lattice and spin-spin relaxation times.

With the proper substitutions, an expression for the ratio I/Io can then be derived for mean velocities ($\bar{v}$) lower or greater, respectively,

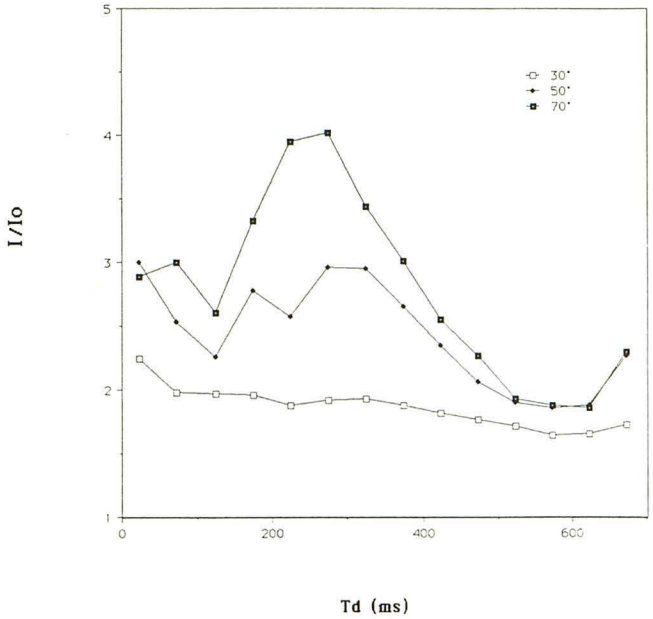

Fig. 7.—Experimental verification of fast multiphase MR signal dependence on flip angle in the case of pulsatile flow. Signal intensity of flowing fluid, averaged over conduit cross section and normalized to signal of surrounding static fluid (I/Io), is plotted vs delay time (Td) from simulated R wave for three different flip angles (30°, 50°, and 70°) and pump rate of 60 cycles/min. A 70° pulse gives a higher enhancement and provides a more sensitive demonstration of flow variations.

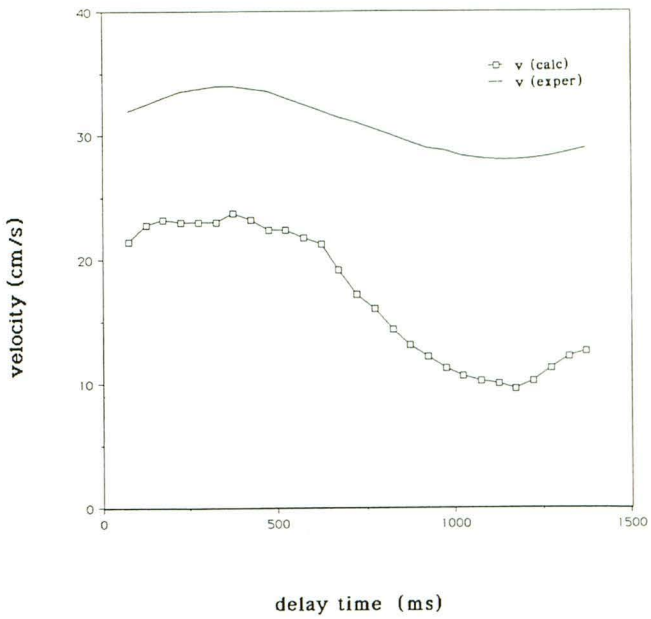

Fig. 8.—Comparison between effective flow vs time curve, and corresponding velocity data derived from fast multiphase imaging (FMI) signal measurements in a pulsatile flow phantom. Similar variations during a pump period are observed. Flow rates calculated from FMI signal are, however, underestimated and the range between actual minimum and maximum values is greater than that indicated by flowmeter. v(calc) = calculated flow rate; v(exper) = experimental flow rate.

than $\Delta z/2\tau$:

$$I/Io = 1 + (\tau/\Delta z)[\exp(-TE/T2)/Io - 1]\bar{v}$$

for $\bar{v} \leq \Delta z/2\tau$, and

$$I/Io = \exp(-TE/T2)/Io + (\Delta z/4\tau\bar{v})[1 - \exp(-TE/T2)/Io]$$

for $\bar{v} \geq \Delta z/2\tau$. If plotted vs mean velocity for certain acquisition parameters, I/Io shows a sharp linear increase and a saturation level is then reached smoothly. In Figure 5 the plot refers to the following acquisition parameters: slice thickness = 6 mm, heart phase interval = 50 msec, T1 ≅ 2000 msec, and flip angle = 70°.

Experimental Model

The dependence of FMI signal on flow rate and, additionally, on the excitation pulse flip angle has been tested in a phantom in the case of both continuous and pulsatile flow.

An artificial circulation was set up, including an electromechanical pump that can be driven in both continuous and pulsatile modes, a cylindrical phantom with elastic inlet and outlet conduits (2 cm in diameter), and an electromagnetic flowmeter. The latter detects a signal from an electrically conductive disk of fluid (in our case a 3-mmol/l copper sulfate aqueous solution). The signal is sampled at a frequency of about 3 Hz and then converted to digital form. The flow rate is thus recorded and displayed on the monitor. A pressure transducer connected to the inlet arm of the phantom monitors the pressure behavior of the flowing fluid. In the case of pulsatile flow, the detected flow signal can be adjusted to replace the ECG signal and transmitted to the cardiac gating apparatus. Therefore, data acquisition can be synchronized to a certain moment of the pump cycle.

The phantom images were obtained with the use of a 0.5-T MR scanner (Philips Gyroscan). The FMI sequences used variable flip angles, a 50-msec interval between serial excitations (τ), and a TE of 8 msec. Reconstruction of a 15-mm-thick transverse slice was done by 2DFT on a 400 × 400 mm field of view with a 128 × 128 matrix.

A substantial agreement (about a 17% difference) was found between theoretical predictions of flow rate (Fig. 5) and experimental data in the case of a steady flow (Fig. 6). This result is in keeping with that recently reported by others [10]. Moreover, the flow-related enhancement proved to be more pronounced with increasing excitation-pulse flip angles.

Driving the pump in a pulsatile mode, a 70° pulse turned out to give a higher flow enhancement, providing a more sensitive demonstration of flow variations during the pump cycle (Fig. 7). Figure 8 shows the comparison between the effective flow vs time curve, measured by the flowmeter, and the corresponding velocity data computed from the signal behavior in the case of pulsatile flow. Similar variations were observed during a pump period. The flow rates calculated from the FMI signal, however, are underestimated, and the range between the actual minimum and maximum values is greater than that measured experimentally. This precludes any system calibration.

To our knowledge, experimental data on the gradient-echo signal dependence on flow rate in the case of pulsatile flow are not currently available in the literature.

ACKNOWLEDGMENTS

We thank Massimo Baroni and Loriana Bendoni for technical assistance.

REFERENCES

1. Sherman JL, Citrin CM. Magnetic resonance demonstration of normal CSF flow. *AJNR* **1986**;7:3–6
2. Bradley WG Jr, Kortman KE, Burgoyne B. Flowing cerebrospinal fluid in normal and hydrocephalic states: appearance on MR images. *Radiology* **1986**;159:611–616
3. Bergstrand G, Bergstrom M, Nordell B, et al. Cardiac gated MR imaging of cerebrospinal fluid flow. *J Comput Assist Tomogr* **1985**;6:1003–1006
4. Citrin C, Sherman JL, Gangarosa RE, Scanlon D. Physiology of the CSF flow-void sign: modification by cardiac gating. *AJNR* **1986**;7:1021–1024
5. Mark AS, Feinberg DA, Brant-Zawadzki MN. Changes in size and magnetic resonance signal intensity of the cerebral CSF spaces during the cardiac cycle as studied by gated, high resolution magnetic resonance imaging. *Invest Radiol* **1987**;22:290–297
6. van der Meulen P, Groen JP, Cuppen JJM. Very fast MR imaging by field echoes and small angle excitations. *Magn Reson Imaging* **1985**;3: 297–299
7. Frahm I, Haase A, Matthaei D. Rapid NMR imaging of dynamic processes using the FLASH technique. *Magn Reson Med* **1986**;3:321–327
8. Nayler GL, Firmin DN, Langmore DB. Blood flow imaging by cine magnetic resonance. *J Comput Assist Tomogr* **1986**;10:715–722
9. Evans AI, Hedlund LW, Herfkens RI, Utz IA, Fram EK, Blindes RA. Evaluation of steady and pulsatile flow with dynamic MRI using limited flip angles and gradient refocused echoes. *Magn Reson Imaging* **1987**;5: 475–482
10. Gao JH, Holland SK, Gore JC. Nuclear magnetic resonance imaging signal from flowing nuclei in rapid imaging using gradient echoes. *Med Phys* **1988**;15:809–914
11. van Dijk P. Multiphase mode and cinedisplay permit dynamic flow MR imaging. *Diagn Imaging* **1986**;10:163–168
12. Bering EA Jr. Choroid plexuses and arterial pulsation of the cerebrospinal fluid. *Arch Neurol Psychiatry* **1955**;73:165–172
13. Laitinen L. Origin of arterial pulsation of cerebrospinal fluid. *Acta Neurol Scand* **1968**;44:168–176
14. Marmarou A, Shulman K, Rosende RM. A nonlinear analysis of the cerebrospinal fluid system and intracranial pressure dynamics. *J Neurosurg* **1978**;48:332–344
15. Portnoy HD, Chopp M, Branch C, Shannon MB. Cerebrospinal fluid pulse waveform as an indicator of cerebral autoregulation. *J Neurosurg* **1982**; 56:666–678
16. Du Boulay GH. Pulsatile movements in the CSF pathway. *Br J Radiol* **1966**;39:255–262
17. Mascalchi M, Ciraolo L, Tanfani G, et al. Cardiac-gated phase MR imaging of aqueductal CSF flow. *J Comput Assist Tomogr* **1988**;12:923–926
18. Atlas SW, Mark AS, Fram EK. Aqueductal stenosis: evaluation with gradient echo rapid MR imaging. *Radiology* **1988**;169:449–453
19. Mascalchi M, Ciraolo L, Bucciolini M, Inzitari D, Arnetoli G, Dal Pozzo G. Fast multiphase MR imaging of aqueductal CSF flow: 2. Study in patients with hydrocephalus. *AJNR* **1990**;11:597–603